Title	Point heat sink induced by droplet train impingement
Author(s)	Qiu, Lu; Dubey, Swapnil; Choo, Fook Hoong; Duan, Fei
Citation	Qiu, L., Dubey, S., Choo, F. H., & Duan, F. (2017). Point heat sink induced by droplet train impingement. Applied Physics Letters, 110(19), 191903-.
Date	2017
URL	http://hdl.handle.net/10220/42566
Rights	© 2017 American Institute of Physics (AIP). This paper was published in Applied Physics Letters and is made available as an electronic reprint (preprint) with permission of American Institute of Physics (AIP). The published version is available at: [http://dx.doi.org/10.1063/1.4983463]. One print or electronic copy may be made for personal use only. Systematic or multiple reproduction, distribution to multiple locations via electronic or other means, duplication of any material in this paper for a fee or for commercial purposes, or modification of the content of the paper is prohibited and is subject to penalties under law.

Point heat sink induced by droplet train impingement

Lu Qiu,[1,2] Swapnil Dubey,[2] Fook Hoong Choo,[2] and Fei Duan[1,a)]
[1]School of Mechanical and Aerospace Engineering, Nanyang Technological University, 50 Nanyang Avenue, Singapore 639798
[2]Energy Research Institute @ NTU, Nanyang Technological University, 1 Cleantech Loop, 06-04 Cleantech One, Singapore 637141

(Received 29 March 2017; accepted 2 May 2017; published online 10 May 2017)

A point heat sink is produced by impinging a high frequency microscale droplet stream onto a superheated copper substrate. Although the overall target surface area is larger than the liquid-solid interface by two or three orders of magnitude, the thermal energy is mainly removed through the point heat sink rather than the rest dry area. Therefore, the spherical conduction patterns in the solid materials are observed with a "nozzle-shifting" method which requires only two temperature probes. The temperature gradient in the vicinity of the impingement stagnation point is tremendously high, suggesting that the liquid-solid interface temperature is significantly lower than the far-field bulk temperature of the substrate. Moreover, the liquid-to-solid heat transfer is measured, which agrees well with the theoretical prediction. The maximum interface heat flux can reach around 80 W/mm^2. It is insensitive to the substrate temperature in a relatively wide temperature range, which brings conveniences to the potential industrial applications. *Published by AIP Publishing.*
[http://dx.doi.org/10.1063/1.4983463]

In the modern power-dense electronic devices, a massive amount of thermal energy is produced from a small area,[1] which may generate a "hot spot." It would be helpful to precisely cool the device with a point heat sink, where the thermal energy could be sunk into a spot as well. One solution could be impinging the high frequency micro-sized droplet train onto the hot substrate because a high heat transfer rate was measured inside the impingement induced craters on the non-boiling surfaces.[2,3] The flow and heat transfer characteristics of single[4] and multiple[5] droplet streams were investigated. Similarly, the crown propagation and the associated high heat flux were observed on a superheated substrate due to the continuous surface wetting of the droplet stream.[6,7] The surface pattern influenced the spreading characteristics[8] and postponed the Leidenfrost temperature.[9,10] Once the Leidenfrost point was reached, a stable vapor film was generated which made the surface slithery[11] and the heat transfer worse.[12] For an infinite homogeneous solid block, the point heat sink could generate a spherical heat conduction pattern. Therefore, a phenomenal temperature gradient is anticipated in the vicinity of the sink. In this work, we design an experiment to measure the temperature profile in the substrate with any desired resolution, based on which we can prove that a point heat sink is established.

In the experiments, we impinged a high frequency water droplet train (40 000 Hz), which was generated from a micro nozzle equipped with a piezoelectric vibrator, onto a large copper substrate. The mean droplet diameter, d, and velocity, U, were 0.120 ± 0.004 mm and 14.9 ± 0.5 m/s according to the measurements from the captured images. The Weber number, $We = \rho U^2 d/\sigma$, and the Reynolds number, $Re = \rho U d/\mu$, of the droplets were 371 and 2015, respectively, where ρ, μ, and σ are the density, viscosity, and surface tension of the droplets at ambient temperature. The circular target surface had a diameter of 20 mm which was larger than the diameter of the liquid-solid interface, D, by two or three orders of magnitude. It was furnished by a #1200 sandpaper, which resulted in a surface roughness of around 0.11 μm. The copper block was heated by the cartridge heaters at the bottom. All the experiments were conducted in a lab with the temperature of $26 \pm 1\,^{\circ}$C, the pressure of 1 atm, and the relative humidity of $48 \pm 5\%$. The droplet diameter, droplet velocity, and wetted area were measured with Matlab V7.13 from the images captured with a Phantom V711 high-speed camera.[13] The resolution of the captured image was 1024×512 pixel (3.97 μm/pixel). In order to measure the solid temperature with thermocouples, two blind holes were drilled from the side wall: $H_1 = 2$ mm and $H_0 = 7$ mm below the top surface, respectively. In order to measure the temperature difference between the two points, ΔT, a differential K-type thermocouple was employed, which was converted from the voltage output, V_{tc}. A single-ended calibrated K-type thermocouple was inserted in the hole with the depth of H_0 in order to measure the reference temperature, T_{ref}. The diagram of the experimental configuration is illustrated in Fig. 1(a). A typical hydraulic pattern of the liquid is sketched in Fig. 1(b). Normally, the high-velocity splashed secondary droplets do not land on the copper surface again.[6]

If a large number of thermocouples were arranged in the different depths to record the temperature profiles, the conduction pattern could be influenced by drilling many holes to hold the thermocouples. Therefore, we propose a "nozzle-shifting" method to measure the high-resolution temperature profile with only two thermocouples. We fix the temperature sensors but move the nozzle in the X-direction from $X = 0$ mm to 9 mm with an interval of 1 mm. In the experiments, we continuously conduct the measurements from low to high substrate temperature at each location, then cool down the copper substrate, and repeat the experiment at the next point. The variations of the voltage output of the

a)Electronic mail: feiduan@ntu.edu.sg

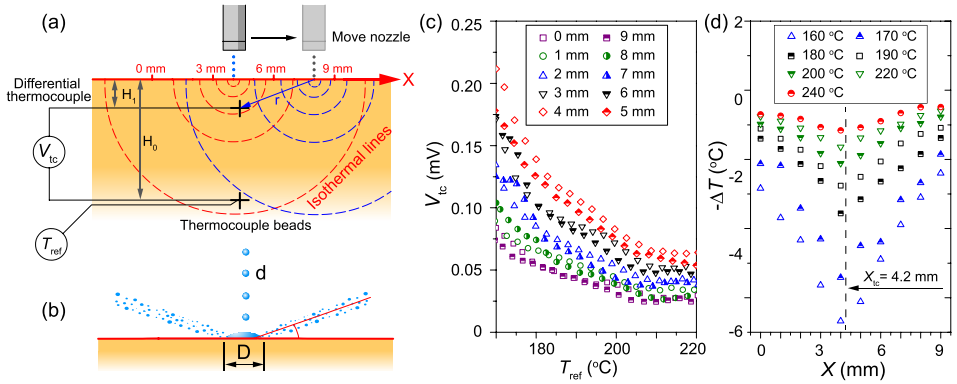

FIG. 1. (a) The experimental method. A differential thermocouple measures the temperature difference (converted from the voltage output) between the two points below the top surface. The temperature of the lower point is measured using a separated thermocouple as the reference. After each set of measurements, the surface is cooled down and the nozzle is horizontally shifted by 1 mm to conduct the next set. (b) A stable wetted area, with a diameter D, could be established at the high substrate temperatures.[6] (c) The variations of the voltage output of the differential thermocouple when the droplet train impinges onto different locations of the copper substrate. (d) The temperature differences measured by the differential thermocouple. A sunken point in the middle of the surface is observed.

differential thermocouple are illustrated in Fig. 1(c). In general, the voltage output decreases with an increase in the reference temperature of the copper block due to the dramatic decrease in the contact area. However, the location of the stagnation point significantly influences the voltage output. When it moves from $X = 0$ to 9 mm, the voltage output increases at first and then decreases after the maximum value measured at $X = 4$ mm. Figure 1(d) shows the variations of the converted temperature difference, ΔT, against X at the different substrate temperatures with a resolution of 1 mm. Higher resolutions could be reached by simply moving the nozzle with the smaller steps. The symmetrical patterns are observed and the center line is close to 4.2 mm, indicating that the thermocouple beads are located at $X_{tc} = 4.2$ mm. Since the data at different X in each group are gathered from ten individually repeated experiments, the orderly variation indicates a good repeatability of the data. A sunken point in the middle of the surface is observed, suggesting that a point heat sink at the top surface exists. However, the quantitative evidence of the spherical conduction pattern is required.

We use spherical coordinates in the following analysis, and the variable r is the radius from the stagnation point [see Fig. 1(a)]. Given that the wetted area has a diameter D, the temperature profile would not be spherical in the near-field of the stagnation point ($r < D/2$) but should be in the mid or far-field ($r > D/2$). If so, we have the steady-state heat equation written as

$$\frac{d}{dr}\left(\lambda r^2 \frac{dT}{dr}\right) = 0, \tag{1}$$

where λ is the thermal conductivity. Thus, the temperature varies with the radius as

$$T(r) = C_1 r^{-1} + C_2, \tag{2}$$

where C_1 and C_2 are two constants. The temperature difference between an interested point (with a radius of r) and the reference point (with a radius of r_{ref}) is

$$\Delta T = T - T_{ref} = C_1(r^{-1} - r_{ref}^{-1}). \tag{3}$$

Once a far-field point is taken as the reference, we have $\Delta T \propto r^{-1}$. Figure 2 reveals the relationship between the measured ΔT and r. The radius is calculated from the thermocouple depth and the horizontal location as $r = \sqrt{H_1^2 + (X - X_{tc})^2}$. Then, we fit each set of data with the power law as $\Delta T = C_1 r^n$, and the fitting constants C_1 and n are illustrated in the inset of Fig. 2. It shows that the exponent n approaches to -1 in a wide range of substrate temperatures, indicating that the spherical heat conduction assumption is reasonable. Since the temperatures are measured in the mid or far-field, the droplet size plays no significant role in the experiments. If we extrapolate the curve to the stagnation point, a significant temperature gradient is predicted. As mentioned, the heat conduction pattern in the near-field should be no longer spherical, so the real liquid-solid interface temperature is difficult to be obtained in the current stage.

More importantly, it is indicated that an extraordinary temperature gradient may be generated in the vicinity of the interface if a low thermal conductivity substrate is employed. For example, as shown in Fig. 2, a temperature difference of 2 °C is generated between $r = 1$ and 2 mm when the copper block temperature is $T_{ref} = 200$ °C (where $D \approx 0.5$ mm). However, it is

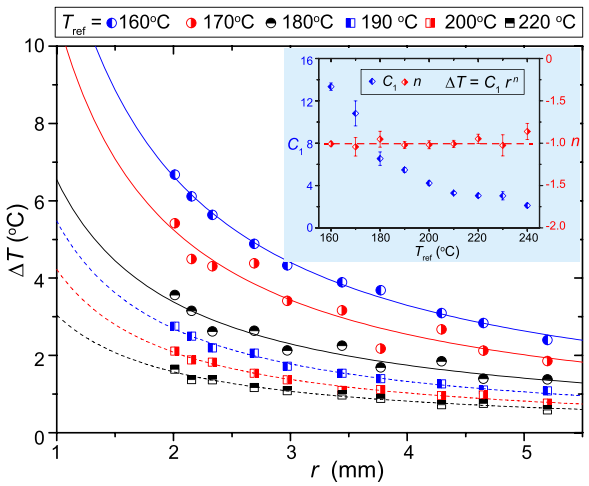

FIG. 2. The variations of the temperature difference in terms of the radius from the stagnation point. The temperature profiles follow the spherical conductive heat transfer pattern $\Delta T = C_1 r^{-1}$. The inset shows the fitting constants.

estimated that the difference could be enlarged to around 40 °C if the substrate thermal conductivity is 20 W/m °C. Therefore, a significant bias may be generated if the surface temperature was not suitably measured. In many recent works, the transparent substrates were employed in the experiments in order to optically measure the liquid-solid contact area or the vapor layer thickness. However, these substrates normally have the lower thermal conductivities compared with copper ($\lambda \approx 400$ W/m °C), such as the glass plate ($\lambda \approx 0.8$ W/m °C) (Ref. 14) or the sapphire plate ($\lambda \approx 23.1$ W/m °C) (Refs. 15–17). The silicon substrate has a relatively high thermal conductivity ($\lambda \approx 148$ W/m °C),[18] but the nano-tube on the top may increase the thermal resistance significantly and decrease the effective thermal conductivity.[19] In those transient experiments, the droplet could only cool down the thin layer below the wetted area in a short period with such low thermal conductivity of the substrate. Therefore, the measured substrate temperature (which could be considered as the far-field) should be significantly different from the real solid-liquid interface temperature. In this case, the Leidenfrost temperature might be significantly overestimated.

The droplet-to-substrate heat transfer is then calculated. Based on the temperature profile described in Eq. (2), the heat flux in the radial direction can be expressed using Fourier's law

$$q(r) = -\lambda \frac{dT}{dr} = \lambda C_1 r^{-2}. \tag{4}$$

Integrating the heat flux on a semi-spherical isothermal surface with an area of $A_s = 2\pi r^2$, we can calculate the cooling power, Q, which is independent of radius due to the energy conservation

$$Q = \oint_{A_s} q(r)\, dA = 2\pi\lambda C_1. \tag{5}$$

The inset of Fig. 2 shows the variation of C_1, from which we can calculate Q. However, a series of experiments are required to fit the curve. Alternatively, we use the following method to find out the transferred energy, where the scan of the droplet train across the surface is not required. Substituting Eq. (3) to replace C_1, we have

$$Q = \frac{2\pi\lambda}{r_1^{-1} - r_0^{-1}} \Delta T = \frac{2\pi\lambda}{S\left(r_1^{-1} - r_0^{-1}\right)} V_{tc} = C_3 V_{tc}, \tag{6}$$

where r_1 and r_0 are the radii of two temperature collection points, and $S = V_{tc}/\Delta T$ is the Seebeck coefficient of the K-type thermocouple. It is shown that the heating power changes linearly with the voltage output of the differential thermocouple, and the slope, C_3, is expressed as

$$C_3 = \frac{2\pi\lambda}{S\left(r_1^{-1} - r_0^{-1}\right)}. \tag{7}$$

Theoretically, the coefficient C_3 can be determined based on the locations of thermocouple beads, the thermal conductivity of the substrate, and the Seebeck coefficient of the thermocouple. For example, when the stagnation point is in line with the thermocouple beads ($X = X_{tc}$), it is predicted from

$$C_{3,pred} = \frac{2\pi\lambda}{S\left(H_1^{-1} - H_0^{-1}\right)}. \tag{8}$$

The predicted slope, $C_{3,pred}$, is presented in Fig. 3, where the uncertainty is mainly generated by the horizontal and vertical displacements of thermocouple beads.

Alternatively, we carried out a series of experiments to calibrate the coefficient, $C_{3,exp}$, with the measured Q_{net} and V_{tc}, in which the required electrical power is tuned to balance the heat removal at different wall temperatures

$$C_{3,exp} = \frac{Q_{net}}{V_{tc}} = \frac{Q_{ele} - Q_{loss}}{V_{tc}} = \frac{Q_{ele} - \beta(T_{ref} - T_e)}{V_{tc}}. \tag{9}$$

The net cooling power, Q_{net}, is obtained by deducting the heat loss, Q_{loss}, from the electric power Q_{ele}. The heat loss includes all the conductive, convective, and radiative losses to the environment. It is calculated from the heat-loss coefficient, β, copper block temperature, T_{ref}, and ambient temperature, T_e. The heat loss coefficient is calibrated from a separate experiment (marked with *) without the droplet impingement. The electrical power is balanced with the heat losses, so the heat-loss coefficient can be calculated as $\beta = Q^*_{ele}/(T^*_{ref} - T^*_e)$. Since the percentage of the heat loss rockets up at high temperature due to the reduction of the net heat transfer, the large deviations are observed at high substrate temperature. As shown in Fig. 3, the best fit of the experimental data agrees well with the prediction in general.

The merit of the second method is that the coefficient, $C_{3,exp}$, could be determined without knowing the locations of thermocouple beads, the thermal conductivity of substrate, or the Seebeck coefficient of the thermocouple. If the stagnation point is moved far away from the thermocouple beads, a high $C_{3,exp}$ could be calibrated. Once the calibration is done, the cooling power can be calculated as $Q = C_{3,exp} V_{tc}$ based on the output of the differential thermocouple. Accompanied by the wetted area, the interface heat flux and heat transfer coefficient could be calculated, as presented in Fig. 4. The wetted diameter is automatically measured using the Matlab image analysis code from the captured images.[6,13] The insets demonstrate the hydrodynamic patterns in three different

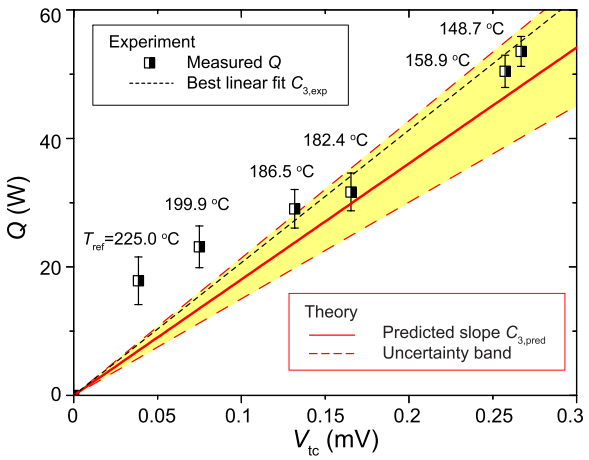

FIG. 3. The cooling power against the voltage output of the differential thermocouple. The coefficient, C_3, is obtained by two mean values, namely, the theoretically predicted $C_{3,pred}$ and the experimentally calibrated $C_{3,exp}$.

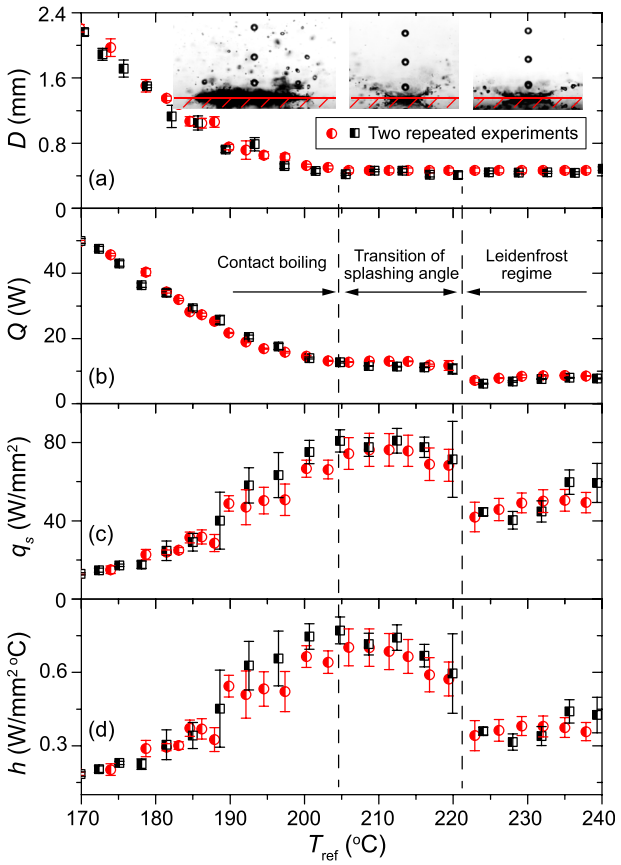

FIG. 4. The variations of (a) wetted diameter captured by the high-speed camera, (b) cooling power, (c) solid-liquid interface heat flux, and (d) heat transfer coefficient. All the experiments are repeated twice. The insets demonstrate the hydrodynamic patterns in three different regimes.

regimes. The interface heat flux and heat transfer coefficient are calculated as $q_s = 4Q/(\pi D^2)$ and $h = q_s/(T_{ref} - T_{sat})$, respectively, where T_{sat} is the boiling temperature of water. Based on the different hydrodynamic patterns and heat transfer characteristics, we define three different regimes, namely, the boiling regime, the transition regime, and the Leidenfrost regime. In the boiling regime, both the cooling power and the wetted area decrease significantly with an increase in substrate temperature. However, the heat flux and the heat transfer coefficient keep increasing because the effects of droplet impingement are dominant when the wetted area is small. In the transition regime, a maximum heat flux of around 80 W/mm^2 is reached. It is insensitive to the copper block temperature in this regime, which gives us the convenience for the potential implementations of the point-cooling concept in the industrial applications. A drastic drop of the heat transfer is distinguished when the Leidenfrost state is established. In this regime, a heat flux reduction of around 50% is measured, but the heat flux itself is still phenomenal. This is different from the heat flux cliff after the critical heat flux in the case of jet impingement boiling. The reason could be inferred that the impingement of the droplets allows the generated vapor to be released periodically so that a stable vapor film, which could significantly undermine the heat transfer, cannot be generated.

In summary, a point heat sink, with a maximum heat flux up to 80 W/mm^2, was generated by impinging the high frequency microscale droplet train on a superheated copper surface. The nozzle-shifting method was developed to measure the high-resolution temperature profiles in the solid substrate, the spherical conduction assumption was subsequently proved, and the interface heat flux was estimated. The maximum heat flux was insensitive to the copper block temperature in a wide range, which gave us the convenience for the potential industrial implementations. Moreover, the temperature gradient close to the wetted area was significantly high even on the copper substrate. It may be instructive for the other droplet impingement related investigations since the Leidenfrost temperature could be significantly overestimated if the substrate temperature was not properly measured, especially in the scenarios of employing the substrates with low thermal conductivity.

This research was supported by the National Research Foundation, Prime Minister's Office, Singapore under the Energy Innovation Programme (NRF2013EWT-EIRP001-017), administered by the Energy Market Authority.

[1]M. A. Ebadian and C. X. Lin, J. Heat Transfer ASME **133**, 110801 (2011).
[2]M. F. Trujillo, J. Alvarado, E. Gehring, and G. S. Soriano, J. Heat Transfer ASME **133**, 122201 (2011).
[3]M. F. Trujillo and S. R. Lewis, Phys. Fluids **24**, 112102 (2012).
[4]T. Zhang, J. P. Muthusamy, J. L. Alvarado, A. Kanjirakat, and R. Sadr, Int. J. Heat Fluid Flow **57**, 24 (2016).
[5]T. Zhang, J. L. Alvarado, J. P. Muthusamy, A. Kanjirakat, and R. Sadr, Int. J. Heat Mass Transfer **110**, 562 (2017).
[6]L. Qiu, S. Dubey, F. H. Choo, and F. Duan, Appl. Phys. Lett. **107**, 164102 (2015).
[7]L. Qiu, S. Dubey, F. H. Choo, and F. Duan, RSC Adv. **6**, 13644 (2016).
[8]A. Alizadeh, V. Bahadur, S. Zhong, W. Shang, R. Li, J. Ruud, M. Yamada, L. Ge, A. Dhinojwala, and M. Sohal, Appl. Phys. Lett. **100**, 111601 (2012).
[9]H.-M. Kwon, J. C. Bird, and K. K. Varanasi, Appl. Phys. Lett. **103**, 201601 (2013).
[10]C. Kruse, T. Anderson, C. Wilson, C. Zuhlke, D. Alexander, G. Gogos, and S. Ndao, Langmuir **29**, 9798 (2013).
[11]P. Dunand, G. Castanet, M. Gradeck, D. Maillet, and F. Lemoine, Int. J. Heat Fluid Flow **44**, 170 (2013).
[12]J. Y. Park, C.-K. Min, S. Granick, and D. G. Cahill, J. Heat Transfer ASME **134**, 101503 (2012).
[13]L. Qiu, S. Dubey, F. H. Choo, and F. Duan, J. Heat Transfer ASME **139**, 052201 (2017).
[14]M. Khavari, C. Sun, D. Lohse, and T. Tran, Soft Matter **11**, 3298–3303 (2015).
[15]H. J. J. Staat, T. Tran, B. Geerdink, G. Riboux, C. Sun, J. M. Gordillo, and D. Lohse, J. Fluid Mech. **779**, R3 (2015).
[16]M. Shirota, M. A. J. van Limbeek, C. Sun, A. Prosperetti, and D. Lohse, Phys. Rev. Lett. **116**, 064501 (2016).
[17]T. Tran, H. J. Staat, A. Susarrey-Arce, T. C. Foertsch, A. van Houselt, H. J. Gardeniers, A. Prosperetti, D. Lohse, and C. Sun, Soft Matter **9**, 3272 (2013).
[18]T. Tran, H. J. Staat, A. Prosperetti, C. Sun, and D. Lohse, Phys. Rev. Lett. **108**, 036101 (2012).
[19]H. Nair, H. J. J. Staat, T. Tran, A. van Houselt, A. Prosperetti, D. Lohse, and C. Sun, Soft Matter **10**, 2102 (2014).